Inorg. Chem. **2006**, *45*, 7709–7721

Trigonal-Bipyramidal Geometry Induced by an External Water Ligand in a Sterically Hindered Iron Salen Complex, Related to the Active Site of Protocatechuate 3,4-Dioxygenase

Takuya Kurahashi,[†] Kenji Oda,[‡] Manabu Sugimoto,[§] Takashi Ogura,[‡] and Hiroshi Fujii*[,†]

Institute for Molecular Science & Okazaki Institute for Integrative Bioscience, National Institutes of Natural Sciences, Myodaiji, Okazaki 444-8787, Japan, and Department of Life Science, Graduate School of Life Science, University of Hyogo, Koto 3-2-1, Kamigori, Ako, Hyogo 678-1297, Japan, and Graduate School of Science and Technology, Kumamoto University, Kumamoto 860-8555, Japan

Received April 17, 2006

A unique distorted trigonal-bipyramidal geometry observed for the non-heme iron center in protocatechuate 3,4-dioxygenase (3,4-PCD) was carefully examined utilizing a sterically hindered iron salen complex, which well reproduces the endogenous His_2Tyr_2 donor set with water as an external ligand. X-ray crystal structures of a series of iron model complexes containing bis(3,5-dimesitylsalicylidene)-1,2-dimesitylethylenediamine indicate that a distorted trigonal-bipyramidal geometry is achieved upon binding of water as an external ligand. The extent of a structural change of the iron center from a preferred square-pyramidal to a distorted trigonal-bipyramidal geometry varies with the external ligand that is bound in the order $Cl \ll EtO < H_2O$, which is consistent with the spectrochemical series. The distortion in the model system is not due to steric repulsions but electronic interactions between the external ligand and the iron center, as evidenced from the X-ray crystal structures of another series of iron model complexes with a less-hindered bis(3-xylylsalicylidene)-1,2-dimesitylethylenediamine ligand, as well as by density functional theory calculations. Further spectroscopic investigations indicate that a unique distorted trigonal-bipyramidal geometry is indeed maintained even in solution. The present model study provides a new viewpoint that a unique distorted trigonal-bipyramidal iron site might not be preorganized by a 3,4-PCD protein but could be electronically induced upon the binding of an external hydroxide ligand to the iron(III) center. The structural change induced by the external water ligand is also discussed in relation to the reaction mechanism of 3,4-PCD.

Introduction

Nature has evolved to produce a variety of metalloenzymes, which play pivotal roles in cooperation with each other.[1] Each metalloenzyme is believed to be specifically designed to carry out a particular chemical reaction assigned to it. Insight into active site structures and the resulting reactions is thus of prime importance from the bioinorganic perspective. In particular, structure−reactivity relationships for mononuclear non-heme iron enzymes are one of the most active areas in recent years.[2] Fueling this interest is an explosion in the number of X-ray crystal structures available for this class of enzymes, which reveal that quite a number of them share a basic coordination motif around the iron center. For example, naphthalene 1,2-dioxygenase, which catalyzes the cis-dihydroxylation of aromatic double bonds, contains a mononuclear iron center coordinated by His208 and His213, bidentately by Asp362, and by a water molecule in a framework comprised of a distorted octahedral bipyramid with one unoccupied coordination site.[3] Other oxygen-activating mononuclear non-heme iron enzymes, such as α-keto acid- and pterin-dependent enzymes, exhibit a similar octahedral iron center that is facially coordinated by two His, one Asp or Glu, and water molecules.[2] The His_2Asp/Glu coordination motif might be required for the generation of a

* To whom correspondence should be addressed. E-mail: hiro@ims.ac.jp.
[†] National Institutes of Natural Sciences.
[‡] University of Hyogo.
[§] Kumamoto University.

(1) For example, see: Lippard, S. J.; Berg, J. M. *Principles of Bioinorganic Chemistry*; University Science Books: New York, 1994.
(2) Costas, M.; Mehn, M. P.; Jensen, M. P.; Que, L., Jr. *Chem. Rev.* **2004**, *104*, 939−986.
(3) Kauppi, B.; Lee, K.; Carredano, E.; Parales, R. E.; Gibson, D. T.; Eklund, H.; Ramaswamy, S. *Structure* **1998**, *6*, 571−586.

10.1021/ic060650p CCC: $33.50
Published on Web 08/25/2006

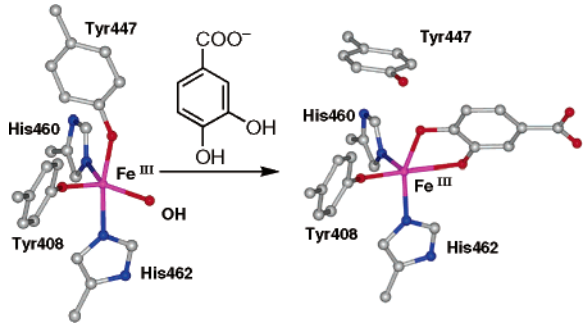

Figure 1. Resting 3,4-PCD and the 3,4-PCD/catecholate complex, created with coordinates obtained from PDB files 2PCD and 3PCA.

key oxoiron(IV) intermediate, as suggested from recent model studies.[4,5]

In contrast, protocatechuate 3,4-dioxygenase (3,4-PCD), which is classified as an intradiol catechol dioxygenase, contains a distinctively different mononuclear non-heme iron center,[6] although an extradiol catechol dioxygenase, 2,3-dihydroxybiphenyl 1,2-dioxygenase, falls into the category of enzymes with a His_2Asp/Glu active site.[7] As shown in Figure 1, the resting form of 3,4-PCD exhibits a unique distorted trigonal-bipyramidal ferric iron center with four endogenous protein ligands (3,4-PCD from *Pseudomonas putida*; Tyr408, Tyr447, His460, and His462). Among these ligands, Tyr447 and His462 are located in axial positions and Tyr408 and His460 serve as equatorial ligands. The other equatorial position is occupied by a solvent-derived ligand, which has been shown to be hydroxide.[8] A series of studies of a range of inhibitor and substrate complexes of both wild-type and mutant 3.4-PCD[9] indicate that the oxidation mechanism is also quite different from other oxygen-activating mononuclear non-heme iron enzymes that contain the His_2Asp/Glu active site. The oxidation sequence is initiated by the binding of a catechol substrate, which involves the displacement of not only the equatorial hydroxide but also the axial Tyr447 ligand, as shown in Figure 1.[2,9] It is noteworthy that the iron coordination geometry is altered from a distorted trigonal-bipyramidal to a square-pyramidal geometry. The formation of a bidentate complex with the structural change is critical for the oxidation of a catechol substrate through a characteristic substrate-activation mechanism not an oxygen-activation mechanism, which is usually employed by other mononuclear non-heme iron enzymes.[10] Although details of the oxidation sequence for 3,4-PCD have been studied, structure−function relationships for 3,4-PCD remain unclear. In particular, it is not clear why 3,4-PCD forms a unique distorted trigonal-bipyramidal geometry for the iron-binding site and why the active-site structure is altered during the substrate-binding process. A drastic shift in the Tyr447 residue suggests the possibility that the distorted trigonal-bipyramidal structure may be enforced by the protein structure of 3,4-PCD, and the displacement of the Tyr447 residue induces a structural change in the active site to a square-pyramidal geometry.

To date, a number of model systems have been successfully constructed to mimic the structure and function of 3,4-PCD.[2,11−21] Particularly important in elucidating the oxidation

(4) (a) Grapperhaus, C. A.; Mienert, B.; Bill, E.; Weyhermüller, T.; Wieghardt, K. *Inorg. Chem.* **2000**, *39*, 5306−5317. (b) Rohde, J.-U.; In, J.-H.; Lim, M. H.; Brennessel, W. W.; Bukowski, M. R.; Stubna, A.; Münck, E.; Nam, W.; Que, L., Jr. *Science* **2003**, *299*, 1037−1039. (c) Lim, M. H.; Rohde, J.-U.; Stubna, A.; Bukowski, M. R.; Costas, M.; Ho, R. Y. N.; Münck, E.; Nam, W.; Que, L., Jr. *Proc. Natl. Acad. Sci. U.S.A.* **2003**, *100*, 3665−3670. (d) Balland, V.; Charlot, M.-F.; Banse, F.; Girerd, J.-J.; Mattioli, T. A.; Bill, E.; Bartoli, J.-F.; Battioni, P.; Mansuy, D. *Eur. J. Inorg. Chem.* **2004**, 301−308. (e) Kaizer, J.; Klinker, E. J.; Oh, N. Y.; Rohde, J.-U.; Song, W. J.; Stubna, A.; Kim, J.; Münck, E.; Nam, W.; Que, L., Jr. *J. Am. Chem. Soc.* **2004**, *126*, 472−473. (f) Decker, A.; Rohde, J.-U.; Que, L., Jr.; Solomon, E. I. *J. Am. Chem. Soc.* **2004**, *126*, 5378−5379. (g) Rohde, J.-U.; Torelli, S.; Shan, X.; Lim, M. H.; Klinker, E. J.; Kaizer, J.; Chen, K.; Nam, W.; Que, L., Jr. *J. Am. Chem. Soc.* **2004**, *126*, 16750−16761. (h) Ghosh, A.; Tiago de Oliveira, F.; Yano, T.; Nishioka, T.; Beach, E. S.; Kinoshita, I.; Münck, E.; Ryabov, A. D.; Horwitz, C. P.; Collins, T. J. *J. Am. Chem. Soc.* **2005**, *127*, 2505−2513. (g) Kim, S. O.; Sastri, C. V.; Seo, M. S.; Kim, J.; Nam, W. *J. Am. Chem. Soc.* **2005**, *127*, 4178−4179.

(5) Kurahashi, T.; Kobayashi, Y.; Nagatomo, S.; Tosha, T.; Kitagawa, T.; Fujii, H. *Inorg. Chem.* **2005**, *44*, 8156−8166.

(6) (a) Ohlendorf, D. H.; Lipscomb, J. D.; Weber, P. C. *Nature* **1988**, *336*, 403−405. (b) Ohlendorf, D. H.; Orville, A. M.; Lipscomb, J. D. *J. Mol. Biol.* **1994**, *244*, 586−608.

(7) Senda, T.; Sugiyama, K.; Narita, H.; Yamamoto, T.; Kimbara, K.; Fukuda, M.; Sato, M.; Yano, K.; Mitsui, Y. *J. Mol. Biol.* **1996**, *255*, 735−752.

(8) True, A. E.; Orville, A. M.; Pearce, L. L.; Lipscomb, J. D.; Que, L., Jr. *Biochemistry* **1990**, *29*, 10847−10854.

(9) (a) Orville, A. M.; Elango, N.; Lipscomb, J. D.; Ohlendorf, D. H. *Biochemistry* **1997**, *36*, 10039−10051. (b) Orville, A. M.; Lipscomb, J. D.; Ohlendorf, D. H. *Biochemistry* **1997**, *36*, 10052−10066. (c) Elgren, T. E.; Orville, A. M.; Kelly, K. A.; Lipscomb, J. D.; Ohlendorf, D. H.; Que, L., Jr. *Biochemistry* **1997**, *36*, 11504−11513. (d) Frazee, R. W.; Orville, A. M.; Dolbeare, K. B.; Yu, H.; Ohlendorf, D. H.; Lipscomb, J. D. *Biochemistry* **1998**, *37*, 2131−2144. (e) Vetting, M. W.; D'Argenio, D. A.; Ornston, L. N.; Ohlendorf, D. H. *Biochemistry* **2000**, *39*, 7943−7955. (f) Valley, M. P.; Brown, C. K.; Burk, D. L.; Vetting, M. W.; Ohlendorf, D. H.; Lipscomb, J. D. *Biochemistry* **2005**, *44*, 11024−11039.

(10) Que, L., Jr.; Lipscomb, J. D.; Münck, E.; Wood, J. M. *Biochim. Biophys. Acta* **1977**, *485*, 60−74.

(11) (a) Funabiki, T.; Sakamoto, H.; Yoshida, S.; Tarama, K. *J. Chem. Soc., Chem. Commun.* **1979**, 754−755. (b) Funabiki, T.; Mizoguchi, A.; Sugimoto, T.; Tada, S.; Tsuji, M.; Sakamoto, H.; Yoshida, S. *J. Am. Chem. Soc.* **1986**, *108*, 2921−2932. (c) Funabiki, T.; Yamazaki, T.; Fukui, A.; Tanaka, T.; Yoshida, S. *Angew. Chem., Int. Ed.* **1998**, *37*, 513−515. (d) Yamahara, R.; Ogo, S.; Watanabe, Y.; Funabiki, T.; Jitsukawa, K.; Masuda, H.; Einaga, H. *Inorg. Chim. Acta* **2000**, *300*−*302*, 587−596. (e) Ogo, S.; Yamahara, R.; Funabiki, T.; Masuda, H.; Watanabe, Y. *Chem. Lett.* **2001**, 1062−1063. (f) Funabiki, T.; Fukui, A.; Hitomi, Y.; Higuchi, M.; Yamamoto, T.; Tanaka, T.; Tani, F.; Naruta, Y. *J. Inorg. Biochem.* **2002**, *91*, 151−158. (g) Funabiki, T.; Sugio, D.; Inui, N.; Maeda, M.; Hitomi, Y. *Chem. Commun.* **2002**, 412−413. (h) Hitomi, Y.; Higuchi, M.; Tanaka, T.; Funabiki, T. *Inorg. Chim. Acta* **2005**, *358*, 3465−3470. (i) Higuchi, M.; Hitomi, Y.; Minami, H.; Tanaka, T.; Funabiki, T. *Inorg. Chem.* **2005**, *44*, 8810−8821.

(12) (a) Lauffer, R. B.; Heistand, R. H., II; Que, L., Jr. *J. Am. Chem. Soc.* **1981**, *103*, 3947−3949. (b) Heistand, R. H., II; Roe, A. L.; Que, L., Jr. *Inorg. Chem.* **1982**, *21*, 676−681. (c) Heistand, R. H., II; Lauffer, R. B.; Fikrig, E.; Que, L., Jr. *J. Am. Chem. Soc.* **1982**, *104*, 2789−2796. (d) Lauffer, R. B.; Heistand, R. H., II; Que, L., Jr. *Inorg. Chem.* **1983**, *22*, 50−55. (e) White, L. S.; Nilsson, P. V.; Pignolet, L. H.; Que, L., Jr. *J. Am. Chem. Soc.* **1984**, *106*, 8312−8313. (f) Pyrz, J. W.; Roe, A. L.; Stern, L. J.; Que, L., Jr. *J. Am. Chem. Soc.* **1985**, *107*, 614−620. (g) Que, L., Jr.; Kolanczyk, R. C.; White, L. S. *J. Am. Chem. Soc.* **1987**, *109*, 5373−5380. (h) Cox, D. D.; Benkovic, S. J.; Bloom, L. M.; Bradley, F. C.; Nelson, M. J.; Que, L., Jr.; Wallick, D. E. *J. Am. Chem. Soc.* **1988**, *110*, 2026−2032. (i) Cox, D. D.; Que, L., Jr. *J. Am. Chem. Soc.* **1988**, *110*, 8085−8092. (j) Jang, H. G.; Cox, D. D.; Que, L., Jr. *J. Am. Chem. Soc.* **1991**, *113*, 9200−9204. (k) Jo, D.-H.; Que, L., Jr. *Angew. Chem., Int. Ed.* **2000**, *39*, 4284−4287.

(13) (a) Weller, M. G.; Weser, U. *J. Am. Chem. Soc.* **1982**, *104*, 3752−3754. (b) Weller, M. G.; Weser, U. *Inorg. Chim. Acta* **1985**, *107*, 243−245.

(14) Casella, L.; Gullotti, M.; Pintar, A.; Messori, L.; Rockenbauer, A.; Györ, M. *Inorg. Chem.* **1987**, *26*, 1031−1038.

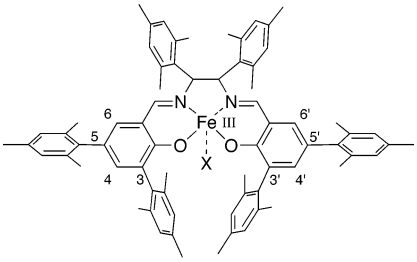

1 (X = Cl), **2** (X = OEt), **3** (X = OH_2), **4** (X = OH)

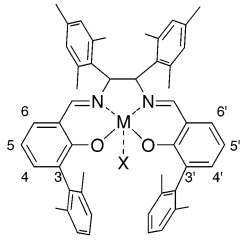

5 (X = Cl, M = Fe^{III}), **6** (X = OMe, M = Fe^{III}),
7 (X = OH_2, M = Fe^{III}), **8** (X = HOMe, M = Fe^{II}),
9 (X = BF_4, M = Mn^{III})

Figure 2. Sterically hindered mesityl iron salen complexes **1**−**4** and less-hindered xylyl salen complexes **5**−**9**.

mechanism of 3,4-PCD are structurally well-defined iron(III) catecholate complexes as models for the enzyme/substrate complex. The reaction of several iron(III) catecholate complexes with O_2 affords intradiol cleavage products in high yield, supporting the proposed substrate-activation mechanism.[11−21] However, no model complex reproducing the distorted trigonal-bipyramidal iron site in resting 3,4-PCD was known until our previous report in 2002.[22] As a model for resting 3,4-PCD, we designed and prepared a sterically hindered salen ligand and successfully obtained the aqua complex **3** (Figure 2), which reproduces the endogenous His_2Tyr_2 donor set with water as an external ligand for 3,4-PCD reasonably well. As previously reported, complex **3** discards the square-pyramidal geometry usually preferred for iron salen complexes and instead adopts a distorted trigonal-bipyramidal geometry that is closely related to the active site in 3,4-PCD, while the geometry of the iron center in the chlorine complex **1** is rather close to a usual square-pyramidal structure. In relation to 3,4-PCD, it is interesting to clarify the driving force for the conversion of a preferred square-pyramidal to a distorted trigonal-bipyramidal geometry in our model system. Herein, we report on an extensive investigation, intended to clarify the electronic and steric effects that lead to a distorted trigonal-bipyramidal geometry in **3**, using a series of sterically hindered mesityl iron salen complexes **1**−**4** and another series of less-hindered xylyl salen complexes **5**−**9**. A close inspection of the X-ray crystal structures of 3,4-PCD and 3,4-PCD-inhibitor complexes in light of the present model study suggests a new possibility that a unique distorted trigonal-bipyramidal iron site might not be preorganized by a 3,4-PCD protein but could be electronically induced upon the binding of an external hydroxide ligand to the iron(III) center.

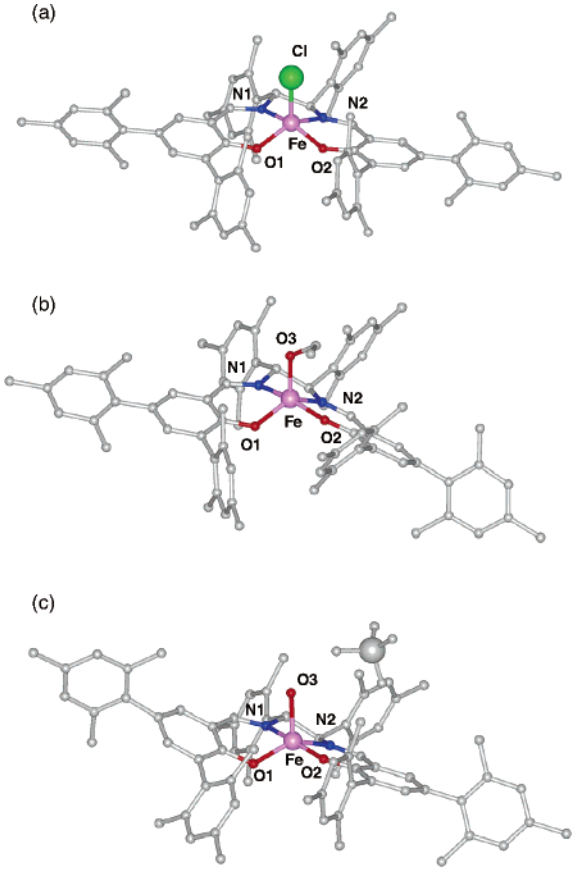

Figure 3. 3-D views for X-ray crystal structures of (a) **1**, (b) **2**, and (c) **3**. Hydrogen atoms and incorporated solvent molecules are omitted for the sake of clarity.

Results

Effect of External Ligands on Distortion around the Iron Center. Figure 3 shows 3-D views of the X-ray crystal structures of **1**−**3**. As reported in the previous paper,[22] **3** shows a unique distorted trigonal-bipyramidal geometry in contrast to the typical square-pyramidal geometry for the chlorine complex **1**. Further inspection of the crystal structure of **3** indicates that the Fe−O (water) bond length in **3** (2.009

(15) (a) Spartalian, K.; Carrano, C. J. *Inorg. Chem.* **1989**, *28*, 19−24. (b) Carrano, C. J.; Carrano, M. W.; Sharma, K.; Backes, G.; Sanders-Loehr, J. *Inorg. Chem.* **1990**, *29*, 1865−1870.
(16) Nishida, Y.; Shimo, H.; Kida, S. *J. Chem. Soc., Chem. Commun.* **1984**, 1611−1612.
(17) Koch, W. O.; Krüger, H.-J. *Angew. Chem., Int. Ed. Engl.* **1995**, *34*, 2671−2674.
(18) (a) Mialane, P.; Anxolabéhère-Mallart, E.; Blondin, G.; Nivorojkine, A.; Guilhem, J.; Tchertanova, L.; Cesario, M.; Ravi, N.; Bominaar, E.; Girerd, J.-J.; Münck, E. *Inorg. Chim. Acta* **1997**, *263*, 367−378. (b) Mialane, P.; Tchertanov, L.; Banse, F.; Sainton, J.; Girerd, J.-J. *Inorg. Chem.* **2000**, *39*, 2440−2444.
(19) (a) Duda, M.; Pascaly, M.; Krebs, B. *Chem. Commun.* **1997**, 835−836. (b) Pascaly, M.; Duda, M.; Schweppe, F.; Zurlinden, K.; Müller, F. K.; Krebs, B. *J. Chem. Soc., Dalton Trans.* **2001**, 828−837. (c) Merkel, M.; Pascaly, M.; Krebs, B.; Astner, J.; Foxon, S. P.; Schindler, S. *Inorg. Chem.* **2005**, *44*, 7582−7589.
(20) Ogihara, T.; Hikichi, S.; Akita, M.; Moro-oka, Y. *Inorg. Chem.* **1998**, *37*, 2614−2615.
(21) (a) Viswanathan, R.; Palaniandavar, M.; Balasubramanian, T.; Muthiah, T. P. *Inorg. Chem.* **1998**, *37*, 2943−2951. (b) Velusamy, M.; Palaniandavar, M.; Gopalan, R. S.; Kulkarni, G. U. *Inorg. Chem.* **2003**, *42*, 8283−8293. (c) Velusamy, M.; Mayilmurugan, R.; Palaniandavar, M. *Inorg. Chem.* **2004**, *43*, 6284−6293. (d) Velusamy, M.; Mayilmurugan, R.; Palaniandavar, M. *J. Inorg. Biochem.* **2005**, *99*, 1032−1042.
(22) Fujii, H.; Funahashi, Y. *Angew. Chem., Int. Ed.* **2002**, *41*, 3638−3641.

Table 1. Bond Distances (Å) and Bond Angles (deg) for **1**−**3**[a]

	1	**2**	**3**
Fe−X	2.234(3)	1.850(5)	2.009(3)
Fe−O1	1.878(5)	1.879(4)	1.863(3)
Fe−O2	1.881(6)	1.869(3)	1.876(3)
Fe−N1	2.087(6)	2.080(4)	2.060(3)
Fe−N2	2.102(6)	2.096(5)	2.084(3)
O1−Fe−N2	143.3(3)	132.6(2)	137.7(1)
O2−Fe−N1	154.1(3)	159.6(2)	166.6(1)
τ	0.18	0.45	0.48

[a] Labeling of the ligand atoms in **1**−**3** is shown in Figure 3.

Å) is longer than those (1.87−1.93 Å) in hydroxide model complexes[23] and the resting state of 3,4-PCD[6] but much shorter than those (2.21−2.30 Å) in the aqua complexes in related model systems.[24] The iron-bound water ligand in **3** seems to be considerably deprotonated via hydrogen-bonding interaction with the ClO_4^- counteranion and is more like hydroxide than water. To evaluate the effect of the external ligand more precisely, an X-ray crystallographic analysis was conducted for the iron complex **2** bearing ethanol as an external ligand in the same mesityl salen framework. As can clearly be seen, the ethanol complex **2** adopts a distorted trigonal-bipyramidal structure similar to that of complex **3**. The structural parameters for **2** are listed in Table 1, compared with those previously reported for **1** and **3**. For a quantitative evaluation of the extent of distortion around the five-coordinate iron center, the geometric parameter τ is employed (eq 1),[25] and the τ values calculated for **1**−**3** are included in Table 1. The τ value can be conveniently utilized to estimate the degree of distortion from square-pyramidal to trigonal-bipyramidal structures. In the case of an ideal square-pyramidal geometry, the τ value is equal to zero, while it becomes unity for a perfect trigonal-bipyramidal geometry.

$$\tau = (\beta - \alpha)/60 \qquad \alpha, \beta: \angle O1-Fe-N2, \angle O2-Fe-N1, \beta > \alpha \quad (1)$$

The τ values for **1**−**3** reveal that the distortion around the iron center is indeed correlated with the external ligand and that the order of distortion upon binding of external ligands is Cl ≪ EtO < H_2O. The order of Cl ≪ EtO < H_2O is identical with that for a well-known spectrochemical series.[1]

Solid-State Studies of Less-Hindered Iron Salen Complexes. As suggested from Figure 3, steric repulsion between the methyl groups at the para positions of the 3- and 3′-mesityl groups in the mesityl salen ligand might induce distortion from a preferred square-pyramidal geometry of the salen framework. Thus, we designed another salen framework bearing xylyl groups at positions 3 and 3′ instead of mesityl groups and prepared **5**−**9** in order to unambiguously examine the effect of the external ligand. The X-ray crystal structures of **5**, **6**, **8**, and **9** in Figure 4 show that there is indeed no steric repulsion between the xylyl groups at the 3 and 3′ positions. Table 2 summarizes selected bond distances and angles.

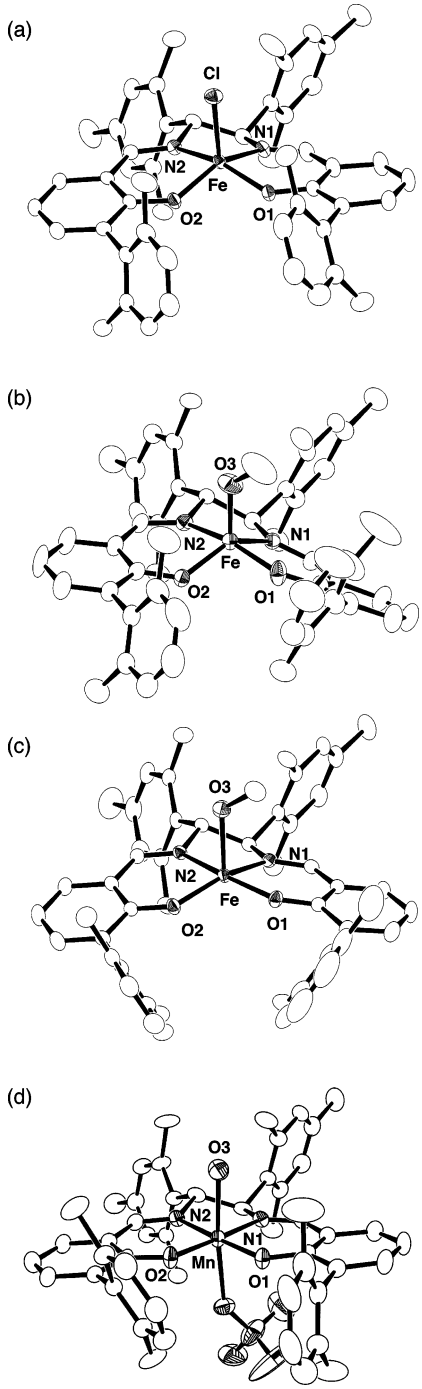

Figure 4. X-ray crystal structures of (a) **5**, (b) **6**, (c) **8**, and (d) **9**. Thermal ellipsoids represent the 50% probability surfaces. Hydrogen atoms and incorporated solvent molecules are omitted for the sake of clarity.

An X-ray crystal structure of the chlorine complex **5** in Figure 4a indicates that **5** contains a square-pyramidal iron center closely resembling that of **1**. Comparison of the τ values shows that **5** ($\tau = 0.16$) is slightly less distorted than

(23) (a) Ogo, S.; Yamahara, R.; Roach, M.; Suenobu, T.; Aki, M.; Ogura, T.; Kitagawa, T.; Masuda, H.; Fukuzumi, S.; Watanabe, Y. *Inorg. Chem.* **2002**, *41*, 5513−5520. (b) MacBeth, C. E.; Gupta, R.; Mitchell-Koch, K. R.; Young, V. G., Jr.; Lushington, G. H.; Thompson, W. H.; Hendrich, M. P.; Borovik, A. S. *J. Am. Chem. Soc.* **2004**, *126*, 2556−2567.

(24) (a) Kennedy, B. J.; Brain, G.; Horn, E.; Murray, K. S.; Snow, M. R. *Inorg. Chem.* **1985**, *24*, 1647−1653. (b) Shyu, H.-L.; Wei, H.-H.; Lee, G.-H.; Wang, Y. *J. Chem. Soc., Dalton Trans.* **2000**, 915−918.

(25) Addison, A. W.; Rao, T. N.; Reedijk, J.; van Rijn, J.; Verschoor, G. C. *J. Chem. Soc., Dalton Trans.* **1984**, 1349−1356.

Table 2. Bond Distances (Å) and Bond Angles (deg) for **5**, **6**, **8**, and **9**[a]

	5	**6**	**8**	**9**
M−X	2.2369(7)	1.840(2)	2.170(2)	2.299(4)
M−O1	1.896(2)	1.890(2)	1.987(2)	1.866(3)
M−O2	1.885(2)	1.894(2)	1.943(2)	1.847(4)
M−N1	2.096(2)	2.112(2)	2.101(2)	1.974(4)
M−N2	2.111(2)	2.094(2)	2.112(2)	1.980(4)
O1−M−N2	153.68(8)	158.38(9)	165.24(7)	175.8(2)
O2−M−N1	144.29(8)	136.92(9)	154.21(8)	174.1(2)
τ	0.16	0.36	0.18	0.03

[a] Labeling of the ligand atoms in **5**, **6**, **8**, and **9** is shown in Figure 4.

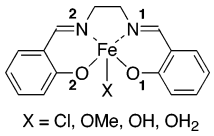

Figure 5. Labeling of the ligand atoms for DFT calculations.

the corresponding chlorine complex **1** ($\tau = 0.18$), probably because of reduced steric repulsion. As shown in Figure 4b, the iron center in the methanol complex **6** exhibits a considerable structural change from a preferred square-pyramidal to a distorted trigonal-bipyramidal geometry ($\tau = 0.36$), compared to the corresponding ethanol complex **2** ($\tau = 0.45$). Unfortunately, the effect of water as an external ligand in the xylyl salen framework could not be investigated because we were unable to obtain crystals of the water complex **7** suitable for an X-ray crystal analysis. However, the distortion around the iron center observed for xylyl iron salens **5** and **6** is exactly parallel to that observed for the mesityl iron salen series. This clearly indicates that the structural change from a square-pyramidal to a distorted trigonal-bipyramidal geometry is not the result of steric repulsions but is induced electronically upon the binding of an external ligand.

A further insight was obtained from the X-ray crystal structure of the iron(II) complex **8** bearing methanol as an external ligand (Figure 4c). As shown in Table 2, the Fe−OMe bond length (2.170 Å) is consistent with the binding of methanol to the ferrous iron center, and the phenolate O−Fe bonds in the iron(II) complex **8** are longer than those in the iron(III) complexes **5** and **6**. The iron center in **8** is rather close to a square-pyramidal geometry ($\tau = 0.18$), suggesting that the electronic effects by external ligands are specific for the iron(III) site. External ligands do not induce any distortion around the manganese(III) center either because the manganese salen complex **9** bearing a weakly bound water as an external ligand shows a square-pyramidal manganese(III) center ($\tau = 0.03$), as shown in Figure 4d.

Density Functional Theory (DFT) Calculations. The electronic nature of the distortion around the iron center was investigated by means of DFT calculations. DFT calculations were conducted for nonsubstituted iron salens with Cl, MeO, OH, and H_2O as an external ligand (Figure 5) to focus particular attention on the electronic interaction between external ligands and the iron center as well as to simplify the system for calculation. Table 3 shows selected parameters for optimized structures of the high-spin complexes ($S = {}^5/_2$). Selected parameters for optimized structures of the intermediate-spin complexes ($S = {}^3/_2$) are listed in Table 4.

Table 3. Bond Distances (Å) and Bond Angles (deg) for Optimized Structures of the High-Spin Complexes ($S = {}^5/_2$)[a]

	X = Cl	X = OMe	X = OH	X = OH_2
Fe−X	2.331	1.827	1.837	2.089
Fe−O1	1.892	1.926	1.920	1.863
Fe−O2	1.898	1.930	1.924	1.873
Fe−N1	2.124	2.127	2.125	2.101
Fe−N2	2.139	2.158	2.158	2.116
O1−Fe−N2	140	137	136	143
O2−Fe−N1	157	157	157	165
τ	0.28	0.33	0.35	0.37

[a] Labeling of the ligand atoms is shown in Figure 5.

Table 4. Bond Distances (Å) and Bond Angles (deg) for Optimized Structures of the Intermediate-Spin Complexes ($S = {}^3/_2$)[a]

	X = Cl	X = OMe	X = OH	X = OH_2
Fe−X	2.376	1.853	1.865	2.176
Fe−O1	1.890	1.934	1.932	1.833
Fe−O2	1.870	1.888	1.882	1.838
Fe−N1	1.941	1.948	1.941	1.943
Fe−N2	1.967	1.997	2.007	1.953
O1−Fe−N2	152	145	142	163
O2−Fe−N1	166	166	168	172
τ	0.23	0.35	0.43	0.15

[a] Labeling of the ligand atoms is shown in Figure 5.

The high-spin complexes are calculated to be more stable than the corresponding intermediate-spin complexes by 0.24 (Cl), 0.42 (MeO), 0.39 (OH), and 0.01 eV (H_2O), which is in agreement with the experimental observation that all of the iron salen complexes investigated herein are in a high-spin electronic state (see the next section). As shown in Table 3, DFT calculations indicate that the coordination of water to the high-spin iron(III) center causes the largest structural change from a square-pyramidal to a distorted trigonal-bipyramidal structure ($\tau = 0.37$). Along with a spectrochemical series of external ligands, the distortion is calculated to become smaller ($\tau = 0.35$ for OH, $\tau = 0.33$ for MeO, and $\tau = 0.28$ for Cl). The order of distortion, as estimated from DFT calculations, is thus exactly the same as the experimental observation. Computationally reproduced distortion in the absence of any steric interaction unambiguously indicates that the distortion around the iron(III) center is induced electronically by the external ligand. It is interesting to note that water coordination to the hypothetical intermediate-spin iron(III) center does not cause such distortion (Table 4), suggesting that the d^5 high-spin electron configuration might be responsible for the unique structural feature of the water complex **3** as a model for 3,4-PCD.

Solution Studies. To further study the structures in solution, we characterized **1**−**7** in dichloromethane using various spectroscopic methods as shown in Table 5. Salen complexes, **1**−**7**, showed quasi-reversible redox peaks at room temperature. The redox potential for Fe^{II}/Fe^{III} is quite sensitive to the external ligand. The chlorine complexes **1** and **5** show the same redox potential at −0.48 V vs SCE,

Table 5. Electrochemical and Spectral Data for **1**−**7**

	1[a]	**2**[a]	**3**[b]	**4**[b]	**5**[a]	**6**[a]	**7**[a]
redox potential $E_{1/2}$ vs SCE/V[c]	−0.48	−1.04	0.00	−0.97	−0.48	−1.09	0.01
UV−vis	460 (7.2)	370 (12.1)	331 (15.3)	363 (11.9)	435 (6.0)	365 (11.8)	335 (16.7)
λ_{max}/nm	516 (7.0)		433 (4.5)		485 (5.0)		490 (4.2)
(ϵ/10^3 M^{-1} cm^{-1})			535 (4.6)				550 (3.9)
^{1}H NMR 5H shifts/ppm[d]					−69.5, −65.6	−47.7	−67.4
6H shifts/ppm	53.7 (76.7[e])	41.6 (63.4[e])	58.3 (80.2)	42.2 (60.2)	56.8	44.0	40.5
	56.1 (80.2[e])		(90.2)				
4H shifts/ppm	85.1 (121.4)	72.9 (103.2)	89.9 (127.4)	73.7 (99.5)	89.7	76.4	79.9
	88.9 (125.7)	(108.6)	(136.0)	(105.5)	91.6		
EPR	8.1 6.7	9.5	9.2	9.4	6.8	9.3	9.4
g	3.5 5.2	4.3	4.3	4.3	5.3	4.3	4.2
(E/D)	1.8 2.0	(0.25)	(0.21)	(0.25)	2.0	(0.23)	(0.24)
	(0.10) (0.03)				(0.03)		
resonance Raman	1310	1316	1304	1327			
ν_{C-O}/cm^{-1}, at 297 K	1340	1340	1338				

[a] UV−vis and EPR spectra were measured in CH_2Cl_2 at 297 and 1.5 K, respectively. Resonance Raman and ^{1}H NMR spectra were measured in CD_2Cl_2. [b] UV−vis and EPR spectra were measured in THF/H_2O (7/3) at 297 and 1.5 K, respectively. Resonance Raman and ^{1}H NMR spectra were measured in CD_2Cl_2. [c] Reduction potentials are determined by cyclic voltammetry at 297 K in CH_2Cl_2 containing 0.10 M tetrabutylammonium perchlorate supporting electrolyte. Conditions: a saturated calomel reference electrode; a glassy carbon working electrode; a platinum-wire counter electrode; scan rate 100 mV s^{-1}. [d] ^{1}H NMR spectra were measured in CD_2Cl_2 at 297 K or at 203 K (in parentheses). [e] The signal is too broad to accurately determine the position.

which is close to those of other ferric salen complexes.[26] **2** and **6**, with RO as an external ligand, show an increased redox potential at −1.04 and −1.09 V, respectively. The water complexes **3** and **7** show a redox potential of around 0.00 V. Although the corresponding xylyl iron salen complex **7** was not characterized by X-ray crystal analysis, the similarity of the redox potential of **7** suggests that the water ligand is coordinated as in **3**. The OH complex **4** shows an increased redox potential at −0.97 V, consistent with coordination of an anionic OH ligand.

The salen complexes, **1**−**7**, show ligand-to-metal charge-transfer (LMCT) bands in a visible region, and the peak positions are also dependent on the external ligand. A red solution of the chlorine complex exhibits two absorption maxima in the visible region at 460 and 516 nm for **1** and at 435 and 485 nm for **5**. In the case of the RO complexes **2** and **6**, the absorption in the visible region is diminished considerably, generating an orange solution (λ_{max} 370 nm for **2** and λ_{max} 365 nm for **6**). Both **3** and **7**, with water as an external ligand, give a purple solution in dichloromethane. UV−vis spectra of **3** and **7**, in the visible region, show two broad absorption maxima extending to 800 nm (λ_{max} 433 and 535 nm for **3** and λ_{max} 490 and 550 nm for **7**).

In ^{1}H NMR spectra, salen complexes, **1**−**7**, show alternative paramagnetic shifts for phenolic protons, as in the case of other monomeric iron(III) salen complexes.[12c,27] According to the previous report, the most downfield-shifted signal is assigned to 4H (4H′), and the other is assigned to 6H (6H′) in the phenolate group (see Figure 2 for the numbering of the phenolate protons). In the case of the xylyl iron salens, the peak assigned to 5H is observed upfield. The chlorine complex **1** shows separate ^{1}H NMR signals for both 4H, 4H′ and 6H, 6H′, indicating that **1** has two distinct phenolate rings in solution. Likewise, the xylyl iron salen complex **5** exhibits separate signals for 4H, 4H′ and 5H, 5H′ but a single signal for 6H, 6H′. On the other hand, the RO complexes **2** and **6**, the H_2O complexes **3** and **7**, and the OH complex **4** show single signals for protons in two phenolate rings at 297 K. However, at 203 K, signals for 4H and 4H′ for those complexes are also observed separately.

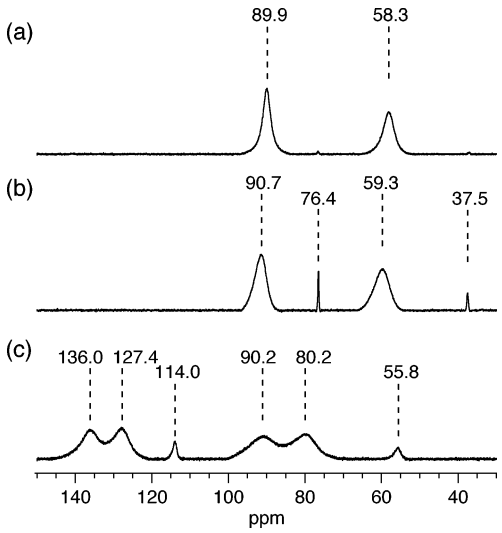

Figure 6. ^{1}H NMR spectra of **3** in wet CD_2Cl_2 at 297 K (a) and in dry CD_2Cl_2 at 297 K (b) and 203 K (c).

Figure 6a shows ^{1}H NMR spectra of **3** in wet CD_2Cl_2 at 297 K. Downfield-shifted signals are observed at 58.3 and 89.9 ppm for **3**, indicating a monomeric iron(III) form in solution. We previously failed to obtain a ^{1}H NMR spectrum at low temperature below 223 K because of extreme line broadening.[22] However, the use of anhydrous aluminum-treated CD_2Cl_2 suppresses line broadening and enables a NMR measurement to be made for the mesityl iron salen series including **3** at 203 K. As shown in Figure 6c, signals for 6H and 4H, which appear at 59.3 and 90.7 ppm as one set of single signals at 297 K, are observed separately at 80.2 and 90.2 ppm (6H) and 127.4 and 136.0 ppm (4H) at 203 K, consistent with **3** having two distinct phenolate rings in solution. In anhydrous CD_2Cl_2, an additional pair of signals of low intensity is observed at 37.5 and 76.4 ppm at 297 K

(26) Lubben, M.; Meetsma, A.; van Bolhuis, F.; Feringa, B. L.; Hage, R. *Inorg. Chim. Acta* **1994**, *215*, 123−129.
(27) La Mar, G. N.; Eaton, G. R.; Holm, R. H.; Walker, F. A. *J. Am. Chem. Soc.* **1973**, *95*, 63−75.

and at 55.8 and 114.0 ppm at 203 K. These signals are readily assigned to H_2O-depleted **3**. In a similar manner, the EtO complex **2** and the OH complex **4** exhibit separated signals especially for 4H, 4H′. On the other hand, the single signals for the xylyl salen complexes were not separated even at low temperature, although the X-ray crystal structures show an asymmetric environment for the two phenolate groups in the salen ligands. This is because of the more rapid pseudorotation of the xylyl salen ligand than the mesityl salen ligand.[28]

Electron paramagnetic resonance (EPR) spectra are also dependent on the external ligand for both the mesityl and xylyl iron salen series. As we recently reported,[5,22] an EPR spectrum of mesityl iron salen **1** shows two sets of signals from high-spin iron(III) centers, a major component with $g = 8.1$, 3.5, and 1.8 ($E/D \approx 0.10$) and a minor component with $g = 6.7$, 5.2, and 2.0 ($E/D \approx 0.03$). On the other hand, the less-hindered xylyl iron salen **5** apparently shows only one set of EPR signals at $g = 6.8$, 5.3, and 2.0 ($E/D \approx 0.03$). Only one set of EPR signals for **5** might indicate a single stable structure in solution for the less-hindered xylyl iron salen complex **5**. The RO complexes show more rhombic EPR signals at $g = 9.5$ and 4.3 ($E/D \approx 0.25$) for **2** and $g = 9.3$ and 4.3 ($E/D \approx 0.23$) for **6**. The H_2O and OH complexes show similar EPR signals at $g = 9.2$ and 4.3 ($E/D \approx 0.21$) for **3**, $g = 9.4$ and 4.2 ($E/D \approx 0.24$) for **7**, and $g = 9.4$ and 4.3 ($E/D \approx 0.25$) for **4**.

1−**3** show two resonance Raman bands, both of which can be assigned to C−O stretching bands, in contrast to a single C−O stretching band at 1337 cm^{-1} reported for the iron salen complex.[12f] As shown in Figure 7a, **3** exhibits two resonance Raman bands at 1304 and 1338 cm^{-1} in CD_2Cl_2 at the excitation wavelength of 457.9 nm. These two bands are also observed at 1306 and 1339 cm^{-1} in the solid state, suggesting that the solid-state structure of **3** is also maintained in solution. As reported for 3,4-PCD,[29] these two bands follow different excitation profiles as shown in Figure 7b. The 1338-cm^{-1} band exhibits a maximum enhancement at around 500 nm, while the 1304-cm^{-1} band approaches a maximum at a wavelength beyond 600 nm. The phenolate with higher energy vibrations gives rise to the higher energy LMCT band. Both **1** and **2**, in addition to **3**, show two resonance Raman bands, further supporting the view that **1**−**3** bear two distinct phenolate rings in solution. The resonance Raman spectrum of **4** shows a single broadened ν_{C-O} band for some as yet unknown reason.

Discussion

Trigonal-Bipyramidal Distortion of Ferric Iron Salen Complexes. The iron salen complex **3** is the first inorganic model complex in which the unique distorted trigonal-bipyramidal ferric iron center in 3,4-PCD is reproduced, as is clearly seen in the X-ray crystal structure and from the τ values in Figure 8. The iron salen complex **3** shares several

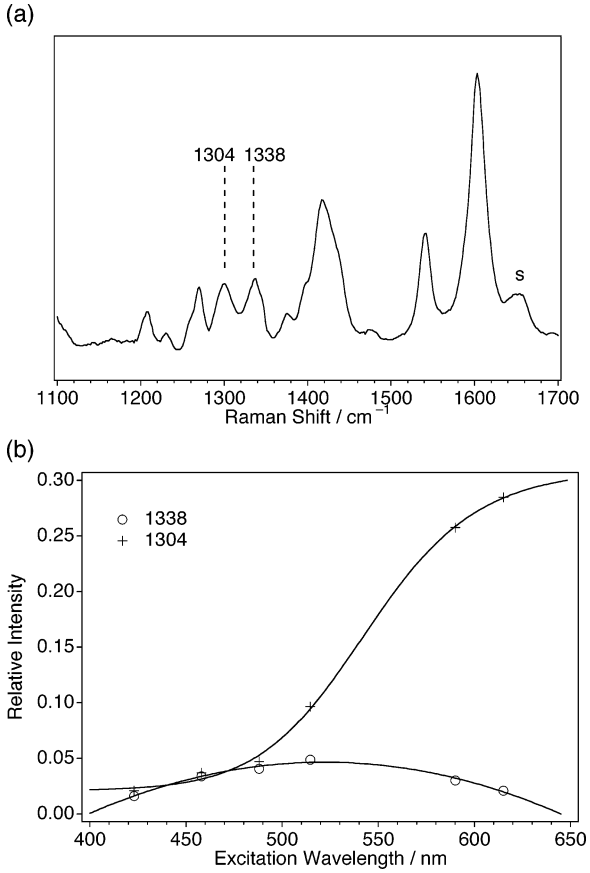

Figure 7. (a) Resonance Raman spectrum of **3** in CD_2Cl_2. The excitation wavelength is 457.9 nm. The band from the solvent is denoted with s. (b) Excitation profiles for the 1304- and 1338-cm^{-1} bands of **3** in CD_2Cl_2. Peak intensities are normalized relative to the 1047-cm^{-1} band from CD_2Cl_2.

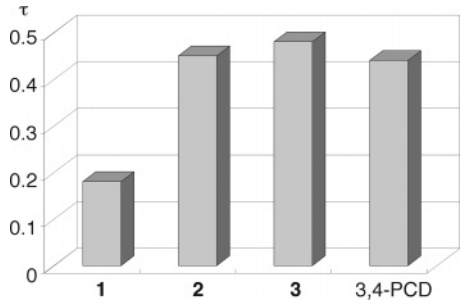

Figure 8. τ values calculated for **1**−**3** in comparison with 3,4-PCD.

other structural characteristics with the active site of the resting state of 3,4-PCD. As reported for 3,4-PCD,[6] **3** has a shorter axial Fe−O2 bond than the equatorial Fe−O1 bond, although the bond length difference of 0.013 Å is smaller than the reported value for 3,4-PCD (0.09 Å). The O2−Fe−N1 angle of 166.6° in **3** is nearly identical with that in 3,4-PCD (167°). The Fe−O(water) bond length in **3** (2.009 Å) is slightly longer than that in 3,4-PCD (1.90 Å). As pointed out in the previous section, however, the iron-bound water ligand in **3** is more like OH than H_2O, considering the previous reports for the Fe−OH (1.87−1.93 Å)[23] and Fe−OH_2 (2.21−2.30 Å)[24] bond lengths in model and enzyme systems. The bond lengths between iron and ligand atoms in 3,4-PCD are longer than those in **3**. Thus, the electron density at the iron(III) center in 3,4-PCD is smaller than that

(28) Berry, R. S. *J. Chem. Phys.* **1960**, *32*, 933−938.
(29) Siu, D. C.-T.; Orville, A. M.; Lipscomb, J. D.; Ohlendorf, D. H.; Que, L., Jr. *Biochemistry* **1992**, *31*, 10443−10448.

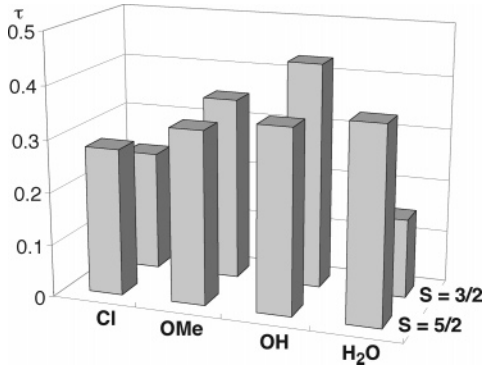

Figure 9. τ values calculated for optimized structures by DFT calculations.

in **3**. The difference in Lewis acidity of the iron(III) center results in the deprotonation of the iron-bound water ligand to form hydroxide in 3,4-PCD but results in partial deprotonation in **3**.

It is generally believed that a salen iron complex consistently maintains a square-pyramidal geometry,[30] and the distorted trigonal-bipyramidal geometry for **3** is unusual and unexpected. It is thus worth discussing in detail the driving force for the unprecedented distortion of the iron(III) salen complex from a preferred square-pyramidal to a unique trigonal-bipyramidal geometry, in the context of structure−reactivity relationships of 3,4-PCD. Figure 8 summarizes the τ values for **1**−**3** in comparison with that for 3,4-PCD. A clear correlation can be seen between distortion and the external ligand, and distortion is increased in the order Cl $\ll$ EtO $<$ H_2O. As was already mentioned, this order is parallel to the spectrochemical series. In other words, as the ligand field of the external ligand of the iron salen complex is stronger, the geometry around the iron center is more distorted to trigonal-bipyramidal. Furthermore, DFT calculations for nonsubstituted high-spin iron salens accurately reproduce the structural distortion of the salen complexes, as shown in Figure 9. A correlation between distortion and the position of the external ligand in the spectrochemical series clearly shows that the distortion is mainly due to electronic interactions between the external ligand and the iron center. In fact, the τ value (0.44) for the resting state of 3,4-PCD is very close to those (0.45 and 0.48) for **2** and **3** (Figure 8). On the other hand, the distortion does not originate from steric repulsion between the *p*-methyl groups of the 3,3′-mesityl groups. This is because the xylyl iron salen complexes **5** and **6** also show a similar trend of distortion.

The electronic configuration of the metal center participates in the creation of a distorted trigonal-bipyramidal structure. The coordination of methanol to the iron(II) center retains a square-pyramidal geometry and the manganese(III) salen complex with the d^4 electronic configuration is not affected at all, even by the water ligand. DFT calculations also indicate that the hypothetical intermediate-spin iron(III) center is not altered to a distorted trigonal-bipyramidal geometry upon the binding of the water ligand (Figure 9). All of these results suggest that a d^5 high-spin configuration is essential for inducing the structural change and that the electron−electron interactions between unpaired electrons in the d orbitals and electrons in the ligand induce this structural change.

The binding of a weak donor ligand at the axial position does not significantly affect the energy levels of the d orbitals of an iron salen complex. However, the binding of a strong donor ligand at the axial position significantly destabilizes some of the d orbitals and increases the total energy of the salen complex. To compensate for the increased total energy, the iron salen complex will tend to stabilize other d-orbital energies via a structural change around the iron. To effectively lower the total energy, the d orbital with the highest energy, $d_{x^2-y^2}$, is stabilized by the distortion of the salen ligand from a preferred square-pyramidal to a trigonal-bipyramidal geometry. Because the ligand-field splits of the d orbitals for iron(II) and manganese(III) salen complexes are smaller than that for the iron(III) salen complex, the effect of the external ligand is not so drastic for the iron(II) and manganese(III) salen complexes. As a result, these complexes show the square-pyramidal geometries, even when a methanol or water ligand is present. For the manganese(III) salen complex, the empty $d_{x^2-y^2}$ orbital no longer contributes to the stabilization.

An insight into the solution structures for **1**−**4** concerning distortion around the iron(III) center is obtained from ^{1}H NMR and EPR data. The ^{1}H NMR spectra of **1**−**4** at 297 K are somewhat contradictory, and in the spectrum of the less distorted **1**, the 6H and 4H signals are separated, although the more distorted **2** and **3** as well as **4** show single signals. This is because the pseudorotation of the salen ligand is relatively slow in the Cl complex **1** compared to the EtO complex **2**, the H_2O complex **3**, and the OH complex **4** at 297 K on the NMR time scale.[28] However, at 203 K, single signals for 4H are clearly separated for **2**−**4** in addition to **1**. Most importantly, the separation between two signals for 4H is on the order of **3** (8.6 ppm) $>$ **4** (6.0 ppm) $>$ **2** (5.4 ppm) $>$**1** (4.3 ppm), suggesting that the structural change from a square-pyramidal to a distorted trigonal-bipyramidal geometry in the solid state also holds for a solution. On the other hand, the fast pseudorotation of the salen ligand suggests that the energy gap between the square-pyramidal and distorted trigonal-bipyramidal structures is very small. EPR spectra of the frozen CH_2Cl_2 solutions of **1**−**4** are also consistent with this because **2** ($E/D \approx 0.25$), **3** ($E/D \approx 0.21$), and **4** ($E/D \approx 0.25$) are much more rhombic than **1** ($E/D \approx$ 0.03 and 0.10). Two ν_{C-O} bands in the resonance Raman spectra indeed indicate two distinct phenolate groups in the iron salen complex but do not appear to reflect the difference in distortion among **1**−**4**.

Relevance to the Structure and Reaction of 3,4-PCD. The present model study reveals a clear correlation between distortion and the position of the external ligand in the

(30) (a) Gerloch, M.; Mabbs, F. E. *J. Chem. Soc. A* **1967**, 1598−1608. (b) Gerloch, M.; Mabbs, F. E. *J. Chem. Soc. A* **1967**, 1900−1908. (c) Gerloch, M.; McKenzie, E. D.; Towl, A. D. C. *J. Chem. Soc. A* **1969**, 2850−2858. (d) Coggon, P.; McPhail, A. T.; Mabbs, F. E.; McLachlan, V. N. *J. Chem. Soc. A* **1971**, 1014−1019. (e) Elerman, Y.; Paulus, H. *Acta Crystallogr., Sect. C* **1996**, *52*, 1971−1973. (f) Elerman, Y.; Kabak, M.; Ülkü, D. *Acta Crystallogr., Sect. C* **1997**, *53*, 712−714.

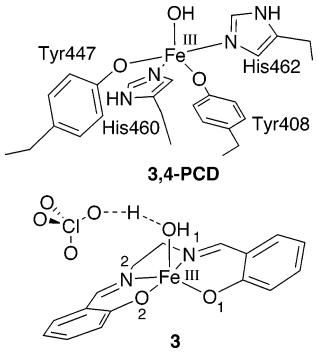

Figure 10. Relevance of the iron salen complex **3** to the active site in resting 3,4-PCD.

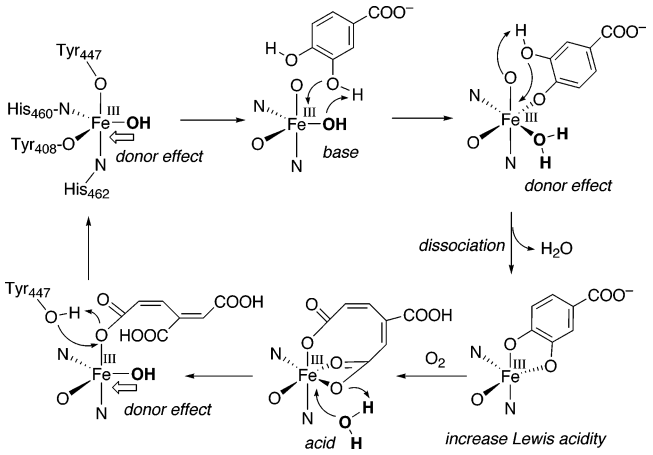

Figure 11. Role of the water ligand on the oxidation process of a catechol substrate by 3,4-PCD.

spectrochemical series and thus unambiguously indicates that a structural change from a square-pyramidal to a distorted trigonal-bipyramidal geometry is electronically induced upon the binding of the external ligand to the iron salen complex. The same electronic effect would be possibly operative in the active site in 3,4-PCD, which bears a N_2O_2 coordination sphere similar to that of the salen complex (Figure 10). The external ligand of the resting state of 3,4-PCD is hydroxide. Although we have not shown the crystal structure of the hydroxide complex **4**, the correlation found in this study suggests that the hydroxide ligand in **4** distorts the iron center to trigonal-bipyramidal geometry as the ethoxide ligand in **2** and the partially deprotonated water ligand in **3**. In fact, as expected from the position of the OH ligand in the spectrochemical series, the τ value for the resting state of 3,4-PCD is closely similar to those for **2** and **3**, as shown in Figure 8. The present ^{1}H NMR study also suggests that **4** has a distorted trigonal-bipyramidal geometry similar to those of **2** and **3** and the distortion is increased in the order of **2** < **4** < **3**. This order is identical with the order expected from the DFT calculations, as well as the spectrochemical series. Close examinations of the X-ray crystal structures of 3,4-PCD further support our proposal for the unique distorted trigonal-bipyramidal geometry. Because there are no steric and strong hydrogen-bonding interactions to the iron-bound hydroxide from protein residues,[6] the hydroxide ligand should be located at the most stable position in energy. Furthermore, as shown by the X-ray crystal structures of 3,4-PCD with various inhibitors, 3,4-PCD is sufficiently flexible to shift the protein ligands to form an octahedral geometry.[9] Although the role of the 3,4-PCD protein on the active-site geometry could not be completely ruled out, all of these findings suggest a new possibility that the unique distorted trigonal-bipyramidal geometry in the 3,4-PCD active site could be electronically induced by the iron(III) center carrying a N_2O_2 coordination sphere with OH as an external ligand. The electronic effect of the hydroxide ligand changes the energies of the iron d orbitals, leading to the ligand shifts to a distorted trigonal-bipyramidal geometry, as observed in this model study.

Figure 11 shows the latest view for the oxidation process of a catechol substrate by 3,4-PCD, which is proposed from a series of X-ray crystal structures of 3,4-PCD[9] as well as a number of model studies.[2,11−21] The previous model studies indicated that the Lewis acidity of the iron center is primarily important for catalysis,[12i,j] while the recent mutagenesis study for 3,4-PCD indicated that efficient catalysis stands on a delicate balance of the Lewis acidity, which must be high enough to promote the charge localization on a catechol substrate necessary for electrophilic O_2 attack yet low enough to allow the necessary ligand rearrangements for rapid turnover.[9f] For the oxidation mechanism of 3,4-PCD, the present results suggest that the electronic effect of the water ligand in the active site of 3,4-PCD controls not only the distorted trigonal-bipyramidal structure of the resting state but also the oxidation process of a catechol substrate. Because of the high Lewis acidity of the iron center of 3,4-PCD, the iron-bound water in 3,4-PCD is deprotonated to a hydroxide. The electronic effect of the iron-bound hydroxide contributes to the trigonal-bipyramidal distortion, as discussed above. The distorted trigonal-bipyramidal geometry may serve to open the binding site for the catechol substrate. The iron-bound hydroxide further acts as a base to accept a proton from the OH group in a catechol substrate, which also assists in the monodentate binding of the substrate. The protonation of the iron-bound hydroxide would weaken the electronic effect, resulting in the conversion of the iron center to an octahedral geometry with substrate binding. This is supported by the X-ray crystal structures of 3,4-PCD phenolic inhibitors and 3,4-PCD under acidic conditions, in which water is still bound to the iron center to form an octahedral geometry.[9e] With the binding of the substrate, the Lewis acidity of the iron center is further decreased by electron donation from the substrate and iron-bound water, which fosters the dissociation of Try447 on binding of the substrate in a bidentate fashion. The formation of the bidentate complex drastically decreases the Lewis acidity of the iron center via an intramolecular electron transfer from the substrate. As a result, the iron-bound water is dissociated. The dissociation of the water ligand is quite important not only to create a site for the subsequent oxygen reaction with the substrate but also to increase the Lewis acidity of the iron center to make it reactive with oxygen as suggested by previous model studies.[12i,j] In fact, the X-ray crystal structural studies show that the water ligand is dissociated with bidentate binding

of a catechol substrate, while it is not dissociated with bidentate binding of an electron-poor inhibitor such as 4-nitrocatechol, 2-hydroxyisonicotinic acid, or 6-hydroxynicotinic acid.[9b,e] The water ligand also plays an important role in the product release process. When the catechol is oxidized to a dicarboxylate compound on the iron center, a water molecule in an active site may facilitate the dissociation of one of the carboxylate moieties from the iron center with protonation. Subsequent binding of the formed hydroxide to the iron center would electronically induce a trigonal-bipyramidal distortion. This accelerates the rebinding of Try447 with dissociation of the other carboxylate moiety, resulting in an efficient release of the product.

Conclusion

Salen iron complexes, which reproduce the unique distorted trigonal-bipyramidal ferric active site in 3,4-PCD, were closely examined with various physicochemical methods. Steric repulsion between introduced mesityl groups in **3** is not the dominant factor in determining geometry, but the binding of an external ligand to the iron(III) center is the key to the unique trigonal-bipyramidal distortion that occurs. An external ligand with a higher position in the spectrochemical series ($Cl \ll RO < H_2O$) induces a larger degree of distortion. As a result of the combination of DFT calculations, we propose that an electronic interaction between the external ligand and the iron center induces the structural change from a preferred square-pyramidal to a distorted trigonal-bipyramidal geometry in the iron(III) salen complex. The present model study provides a new viewpoint for electronic interactions between the external ligand and the central iron(III), which results in a unique distorted trigonal-bipyramidal geometry in 3,4-PCD. The new concept established herein for the construction of a 3,4-PCD model will contribute to revealing the relatively unexplored substrate-binding and product-releasing step by 3,4-PCD.

Experimental Section

Instrumentation. UV−vis spectra were recorded on an Agilent 8453 (Agilent Technologies). 500-MHz ^{1}H NMR spectra were measured on a LA-500 spectrometer (JEOL). Resonance Raman spectra were measured with a quartz spinning cell, maintained at room temperature, using a MC-100DG 100-cm single polychromator (Ritsu Ohyo Kogaku) equipped with an intensified photodiode array (PAR, 1421HQ). An Ar ion laser (NEC, GLG3200) was utilized as an excitation source. The laser power at the sample was about 7 mW. Raman shifts were calibrated with indene. EPR spectra were recorded in a quartz cell (d = 5 mm) at 4 K on an E500 continuous-wave X-band spectrometer (Bruker) with an ESR910 helium-flow cryostat (Oxford Instruments). Elemental analyses were conducted on a CHN corder MT-6 (Yanaco). Cyclic voltammograms were measured with an ALS612A electrochemical analyzer (ALS).

Materials. Ether, tetrahydrofuran (THF), *N*,*N*-dimethylformamide (DMF), dimethoxyethane, methanol, and ethanol were purchased from Kanto Chemical Co., Inc., or Wako Pure Chemical Industries, Ltd., as anhydrous solvents and were stored over 3A or 4A molecular sieves. CD_2Cl_2 was purchased from Acros and was stored in the presence of 4A molecular sieves. CD_2Cl_2 was passed through activated alumina under an argon atmosphere just prior to use. Sodium hydride (60% dispersion in paraffin liquid) was purchased from Nacalai Tesque and was utilized as received. Tetrakis(triphenylphosphine)palladium(0) was purchased from Nacalai Tesque. 2-Mesitylmagnesium bromide (1.0 M in diethyl ether) and 2,6-dimethylphenylmagnesium bromide (1.0 M in THF) were purchased from Aldrich. *n*-Butyllithium (1.6 M in hexane) and *tert*-butyllithium (1.5 M in pentane) were purchased from Kanto Chemical Co., Inc. Alkyllithium concentrations were determined just prior to use according to a previously reported method.[31] Silver tetrafluoroborate (99.99+%) was purchased from Aldrich. Other reagents were purchased from Kanto Chemical Co., Inc., or Wako Pure Chemical Industries, Ltd., and were used as received. ***Caution!*** *The perchlorate salts used in this study are potentially explosive and should be handled in small amounts with great care.*

Scheme 1

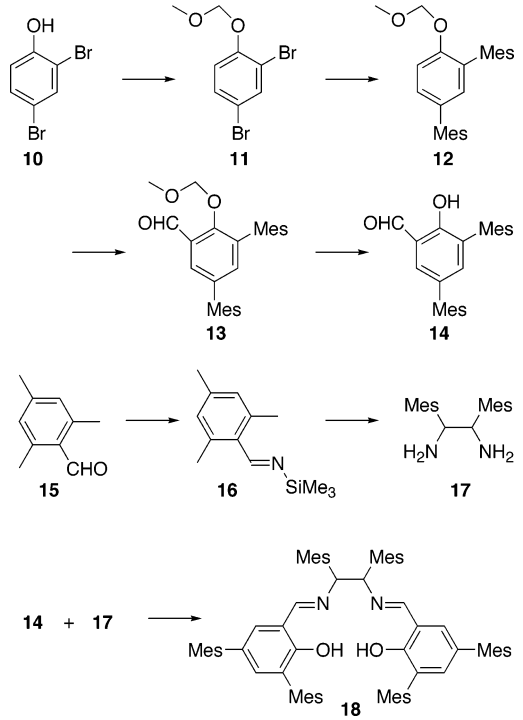

Synthesis of Bis(3,5-dimesitylsalicylidene)-1,2-dimesitylethylenediamine (18). 18 was synthesized according to Scheme 1.

1,3-Dibromo-2-(methoxymethoxy)benzene (11). A solution of **10** (25.53 g, 0.101 mol) in dry ether (50 mL) was added slowly to a suspension of NaH (4.1 g, 0.103 mol) in dry ether (200 mL) and dry DMF (50 mL) under an argon atmosphere. Chloromethyl methyl ether (9.3 mL, 0.122 mol) in ether (10 mL) was then carefully added with vigorous stirring. After 1 h, the solution was quenched with ethanol (10 mL) and then with water (100 mL). The aqueous layer was extracted with ether (100 mL) three times. The combined ether layer was washed with saturated aqueous $NaHCO_3$ (100 mL), distilled water (100 mL), and finally saturated aqueous NaCl (100 mL). The resulting solution was dried over $MgSO_4$ and then evaporated. The residue was purified by vacuum distillation (5 mmHg, 120 °C) to give **11** (20.2 g, 0.068 mol) in 67% yield as an oil. ^{1}H NMR (500 MHz, $CDCl_3$): δ 3.49 (s, 3H), 5.20 (s, 2H), 7.02 (d, J = 8.9 Hz, 1H), 7.33 (dd, J = 2.5 and 8.9 Hz, 1H), 7.66 (d, J = 2.5 Hz, 1H). GC−MS (EI, ether): calcd for $C_8H_8Br_2O_2$ m/z 295.9; found m/z 296.1.

(31) Kofron, W. G.; Baclawski, L. M. *J. Org. Chem.* **1976**, *41*, 1879−1880.

1,3-Dimesityl-2-(methoxymethoxy)benzene (12). Palladium-catalyzed Grignard cross-coupling was employed to incorporate mesityl groups.[32] To a solution of **11** (16.19 g, 54.7 mmol) in dry THF (100 mL) was added tetrakis(triphenylphosphine)palladium (3.27 g, 2.8 mmol) under an argon atmosphere. A 1.0 M solution of 2-mesitylmagnesium bromide in ether (120 mL, 120 mmol) was then slowly added with stirring. After the ether was distilled off upon heating, the solution was refluxed for 12 h. The resulting solution was quenched with careful addition of a 1 M $NaHCO_3$ aqueous solution (100 mL). The aqueous layer was extracted with ether (100 mL) three times. The combined organic layer was washed with saturated aqueous NaCl, dried over $MgSO_4$, and then evaporated. The residue was passed through a silica column (hexane:ethyl acetate = 20:1). Vacuum distillation (1 mmHg, 200 °C) gave pure **12** (10.72 g, 28.6 mmol) in 52% yield as a viscous oil. ^{1}H NMR (500 MHz, $CDCl_3$): δ 2.03 (s, 6H), 2.04 (s, 6H), 2.30 (s, 3H), 2.31 (s, 3H), 3.35 (s, 3H), 5.09 (s, 2H), 6.80 (d, J = 2.1 Hz, 1H), 6.91 (s, 2H), 6.92 (s, 2H), 7.05 (dd, J = 2.1 and 8.6 Hz, 1H), 7.24 (d, J = 8.6 Hz, 1H). GC−MS (EI, ether): calcd for $C_{26}H_{30}O_2$ m/z 374.2; found m/z 374.5.

3,5-Dimesityl-2-(methoxymethoxy)benzaldehyde (13). Ortho-directing lithiation by a methoxymethoxy group is utilized for regioselective incorporation of a formyl group.[33] A 1.59 M solution of *n*-BuLi (17 mL, 27 mmol) was added dropwise with stirring to a solution of **12** (8.43 g, 22.5 mmol) in dry THF (47 mL) at −80 °C under an argon atmosphere. The solution was gradually warmed to −20 °C for 1 h to give a reddish solution. Dry DMF (3.5 mL, 45.2 mmol) was then added at −20 °C, resulting in an immediate color change from reddish to pale orange. After 1 h, the resulting solution was quenched with ethanol (0.5 mL) and then distilled water (120 mL). The aqueous layer was extracted with ether (100 mL) three times. The combined organic layer was washed with saturated aqueous NaCl, dried over $MgSO_4$, and then evaporated. The residue was purified with a silica column chromatography (hexane:ethyl acetate = 20:1) to give **13** (6.18 g, 15.4 mmol) in 68% yield as a white solid. ^{1}H NMR (500 MHz, $CDCl_3$): δ 2.01 (s, 6H), 2.08 (s, 6H), 2.29 (s, 3H), 2.30 (s, 3H), 3.19 (s, 3H), 4.68 (s, 2H), 6.91 (s, 2H), 6.93 (s, 2H), 7.13 (d, J = 2 Hz, 1H), 7.64 (d, J = 2 Hz, 1H), 10.49 (s, 1H). GC−MS (EI, ether): calcd for $C_{27}H_{30}O_3$ m/z 402.2; found m/z 402.4.

3,5-Dimesityl-2-hydroxybenzaldehyde (14). To a solution of **13** (5.45 g, 13.5 mmol) in ethanol (30 mL) was added slowly concentrated HCl (3 mL). The resulting solution was refluxed for 30 min. Then saturated aqueous NaCl (100 mL) was added. The aqueous layer was extracted with ether (100 mL) three times. The combined organic layer was washed with saturated aqueous NaCl, dried over $MgSO_4$, and then evaporated. The residue was purified by silica column chromatography (hexane:ethyl acetate = 20:1) to give **14** (4.82 g, 13.4 mmol) quantitatively as a viscous oil. ^{1}H NMR (500 MHz, $CDCl_3$): δ 2.06 (s, 12H), 2.31 (s, 6H), 6.94 (s, 2H), 6.95 (s, 2H), 7.14 (d, J = 2 Hz, 1H), 7.35 (d, J = 2 Hz, 1H), 9.94 (s, 1H), 11.10 (s, 1H). GC−MS (EI, ether): calcd for $C_{25}H_{26}O_2$ m/z 358.2; found m/z 358.4.

***N*-(Trimethylsilyl)-2,4,6-trimethylbenzylideneimine (16).** This preparation was conducted according to a previously reported procedure.[34] A 1.0 M solution of lithium bis(trimethylsilyl)amide (400 mL, 400 mmol) was added slowly at 0 °C to a solution of **15** (59.3 g, 400 mmol) in dry THF (400 mL) under an argon atmosphere. Particular attention was paid to preventing the solution temperature from exceeding 10 °C. The resulting reddish solution was stirred at 0 °C for 30 min. At room temperature, trimethylsilyl chloride (50 g, 460 mmol) in dry THF (400 mL) was then slowly added. After the solution was stirred for 30 min at room temperature, it was evaporated. The residue was purified by vacuum distillation (1 mmHg, 100 °C) to give **16** (64.8 g, 295 mmol) in 74% yield. ^{1}H NMR (500 MHz, $CDCl_3$): δ 0.24 (s, 9H), 2.26 (s, 3H), 2.38 (s, 6H), 6.83 (s, 1H), 6.84 (s, 1H), 9.32 (s, 1H). GC−MS (EI, ether): calcd for $C_{13}H_{21}NSi$ m/z 219.1; found m/z 219.3.

1,2-Dimesitylethylenediamine (17). The coupling of **16** was carried out in the same manner as the reported procedure.[35] To an orange solution of $NbCl_4(THF)_2$ (52.0 g, 137 mmol) dissolved in dry dimethoxyethane (1.8 L) was added **16** (30.0 g, 137 mmol) in dimethoxyethane (200 mL) under an argon atmosphere. The resulting solution was stirred for 6 h at room temperature, becoming yellow in color. Dimethoxyethane was removed in vacuo, and the residue was treated with 10% aqueous KOH (500 mL) for 20 min. The aqueous layer was extracted with ether (500 mL) three times. The combined organic layer was washed with saturated aqueous NaCl, dried over Na_2SO_4, and then evaporated. The residue was dissolved in methanol, and the addition of water with stirring yielded **17** (26.3 g, 88.7 mmol) in 65% yield as a white solid. ^{1}H NMR (500 MHz, $CDCl_3$): δ 1.62 (s, 6H), 2.16 (s, 6H), 2.65 (s, 6H), 4.70 (s, 2H), 6.52 (s, 2H), 6.78 (s, 2H).

18. To a solution of **17** (1.18 g, 4.0 mmol) in dry methanol (150 mL) was added **14** (2.87 g, 8.0 mmol). The mixture was heated to reflux for 1 h. After cooling, the resulting precipitate was filtered, washed with a small amount of methanol, and dried in vacuo. **18** was obtained in 77% yield as a yellow solid (3.00 g, 3.1 mmol). ^{1}H NMR (500 MHz, $CDCl_3$): δ 1.82 (s, 6H), 1.86 (s, 6H), 1.96 (s, 6H), 1.97 (s, 6H), 2.08 (s, 6H), 2.18 (s, 6H), 2.28 (s, 6H), 2.29 (s, 6H), 2.65 (s, 6H), 5.66 (s, 2H), 6.61 (s, 2H), 6.80 (s, 2H), 6.83 (s, 2H), 6.86 (s, 2H), 6.87 (s, 2H), 6.90 (s, 2H), 6.92 (s, 4H), 8.40 (s, 2H), 13.06 (s, 2H). ^{13}C NMR (125.65 MHz, $CDCl_3$): δ 20.23, 20.31, 20.69, 20.78, 20.84, 20.98, 21.01, 21.13, 22.61, 72.03, 118.92, 127.93, 127.99, 128.46, 129.19, 131.04, 131.15, 131.57, 134.22, 134.33, 134.71, 136.34, 136.41, 136.45, 136.63, 136.76, 137.09, 138.02, 156.57, 165.51. MS (FAB): calcd for $C_{70}H_{77}N_2O_2$ m/z 977.6; found m/z 977.7.

Synthesis of Bis(3-xylylsalicylidene)-1,2-dimesitylethylenediamine (24). 24 was synthesized according to Scheme 2.

Iodo-2-(methoxymethoxy)benzene (20). 20 was synthesized in exactly the same manner as that of **11**. **19** (9.69 g, 44 mmol) was converted to **20** (8.50 g, 32 mmol) in 73% yield as an oil. ^{1}H NMR (500 MHz, $CDCl_3$): δ 3.50 (s, 3H), 5.22 (s, 2H), 6.74 (dd, J = 7.8 and 8.3 Hz, 1H), 7.05 (d, J = 8.3 Hz, 1H), 7.26 (dd, J = 7.6 and 7.8 Hz, 1H), 7.76 (d, J = 7.6 Hz, 1H). GC−MS (EI, ether): calcd for $C_8H_9IO_2$ m/z 264.0; found m/z 264.1.

1-(2,6-Dimethylphenyl)-2-(methoxymethoxy)benzene (21). 21 was synthesized in a manner similar to that of **12**. To a solution of **20** (3.11 g, 11.8 mmol) in dry THF (10 mL) was added tetrakis-(triphenylphosphine)palladium (0.66 g, 0.57 mmol) under an argon atmosphere. Then a 1.0 M solution of 2,6-dimethylphenylmagnesium bromide in THF (16 mL, 16 mmol) was slowly added with stirring. The solution was refluxed for 6 h. The resulting solution was quenched by careful addition of 1 M aqueous Na_2CO_3 (50 mL). The aqueous layer was extracted with ether (50 mL) three times. The combined organic layer was washed with saturated aqueous NaCl, dried over Na_2SO_4, and then evaporated. Vacuum distillation

(32) Tsuji, J. *Palladium Reagents and Catalysts: Innovations in Organic Synthesis*; John Wiley & Sons: Chichester, U.K., 1997.
(33) Winkle, M. R.; Ronald, R. C. *J. Org. Chem.* **1982**, *47*, 2101−2108.
(34) Colvin, E. W.; McGarry, D. G. *J. Chem. Soc., Chem. Commun.* **1985**, 539−540.
(35) Roskamp, E. J.; Pedersen, S. F. *J. Am. Chem. Soc.* **1987**, *109*, 3152−3154.

Scheme 2

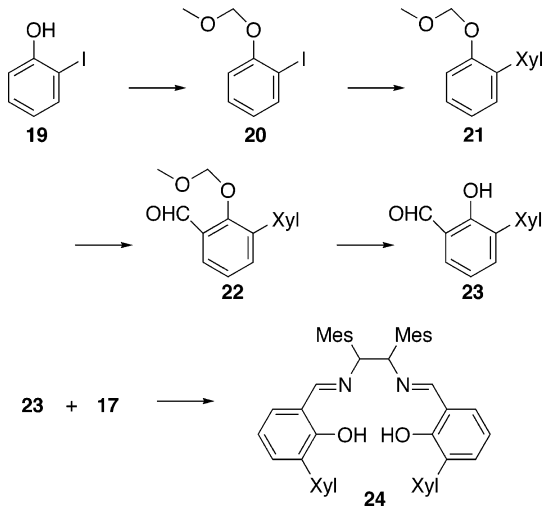

(<1 mmHg, 120 °C) gave pure **21** (2.4 g, 9.9 mmol) in 84% yield as a viscous oil. ^{1}H NMR (500 MHz, $CDCl_3$): δ 2.04 (s, 6H), 3.29 (s, 3H), 5.04 (s, 2H), 7.03 (dd, J = 7.6 and 2.2 Hz, 1H), 7.06 (dd, J = 7.1 and 1.0 Hz, 1H), 7.09 (d, J = 7.9 Hz, 2H), 7.15 (dd, J = 8.6 and 6.6 Hz, 1H), 7.21 (dd, J = 7.3 and 0.8 Hz, 1H), 7.30 (ddd, J = 8.6, 7.3, and 2.2 Hz, 1H). GC−MS (EI, ether): calcd for $C_{16}H_{18}O_2$ m/z 242.1; found m/z 242.2.

3-(2,6-Dimethylphenyl)-2-hydroxybenzaldehyde (23). Regioselective formylation was carried out in a manner similar to that for **13**. A 1.5 M solution of *t*-BuLi (3.5 mL, 5.3 mmol) was added dropwise with stirring to a solution of **21** (600 mg, 2.5 mmol) in dry ether (25 mL) at 0 °C under an argon atmosphere. Dry DMF (510 mg, 7.0 mmol) was then added at 0 °C. After the resulting solution was stirred for 30 min at room temperature, it was quenched with ethanol (25 mL), and 1 M aqueous Na_2CO_3 (50 mL) was then added. The aqueous layer was extracted with ether (50 mL) three times. The combined organic layer was washed with saturated aqueous NaCl, dried over Na_2SO_4, and then evaporated. The residue was passed through a silica column chromatography using toluene as the eluent to give **22**. To a solution of **22** in ethanol (20 mL) was added slowly concentrated HCl (1 mL). The resulting solution was refluxed for 5 min. Then saturated aqueous NaCl (50 mL) was added. The aqueous layer was extracted with ether (50 mL) three times. The combined organic layer was washed with saturated aqueous NaCl, dried over Na_2SO_4, and then evaporated. The residue was purified by silica column chromatography (toluene) to give **23** (550 mg, 2.4 mmol) quantitatively as a viscous oil. ^{1}H NMR (500 MHz, $CDCl_3$): δ 2.03 (s, 6H), 7.10 (dd, J = 7.3 and 7.6 Hz, 1H), 7.12 (d, J = 7.6 Hz, 2H), 7.19 (dd, J = 7.6 and 7.6 Hz, 1H), 7.34 (d, J = 7.3 Hz, 1H), 7.59 (d, J = 7.6 Hz, 1H), 9.96 (s, 1H), 11.13 (s, 1H). GC−MS (EI, ether): calcd for $C_{15}H_{14}O_2$ m/z 226.1; found m/z 226.3.

24. To a solution of **17** (593 mg, 2.0 mmol) in dry methanol (15 mL) was added **23** (910 mg, 4.0 mmol). The mixture was heated to reflux for 1 h. After cooling, the resulting precipitate was filtered, washed with a small amount of methanol, and dried in vacuo. **24** was obtained in 55% yield as a yellow solid (780 mg, 1.09 mmol). ^{1}H NMR (500 MHz, $CDCl_3$): δ 1.69 (s, 6H), 1.84 (s, 6H), 1.95 (s, 6H), 2.17 (s, 6H), 2.65 (s, 6H), 5.61 (s, 2H), 6.59 (s, 2H), 6.81 (s, 2H), 6.83 (dd, J = 7.5 and 7.5 Hz, 2H), 6.96 (dd, J = 1.7 and 7.5 Hz, 2H), 7.04 (d, J = 7.5 Hz, 2H), 7.05 (d, J = 7.5 Hz, 2H), 7.12 (dd, J = 7.6 and 7.6 Hz, 2H), 7.15 (dd, J = 1.7 and 7.6 Hz, 2H), 7.25 (s, 2H), 8.41 (s, 2H). ^{13}C NMR (125.65 MHz, $CDCl_3$): δ 20.24, 20.33, 20.68, 20.77, 22.56, 72.16, 118.50, 118.90, 127.03, 127.05, 127.29, 128.38, 129.23, 131.06, 131.19, 133.39, 133.41, 136.69, 136.87, 136.92, 136.99, 137.34, 157.60, 165.57. MS (FAB) calcd for $C_{50}H_{53}N_2O_2$ m/z 714.0; found m/z 713.5.

Synthesis of Metal Complexes. Syntheses of **1**−**4** are reported elsewhere.[5,22]

5. To a solution of anhydrous $FeCl_3$ (163 mg, 1.0 mmol) in dry ethanol (10 mL) was added **24** (713 mg, 1.0 mmol). The solution was refluxed for 30 min. The resulting dark-red solution was then allowed to stand at room temperature. **5** was obtained in 51% yield as black crystals (410 mg, 0.51 mmol). A crystal suitable for X-ray crystallographic analysis was obtained by recrystallization from acetonitrile. Anal. Calcd for $C_{50}H_{50}N_2O_2ClFe$: C, 74.86; H, 6.28; N, 3.49. Found: C, 74.54; H, 6.42; N, 3.38. IR (KBr): 3449, 3014, 2953, 2920, 2856, 1605, 1555, 1460, 1415, 1384, 1329, 1303, 1270, 1224, 1120, 1090, 1061, 1034, 985, 855, 758, 691, 649, 578 cm^{-1}.

6. To a solution of **5** (401 mg, 0.50 mmol) in methanol (30 mL) was added 0.1 M aqueous NaOH (5 mL). After the resulting red precipitate was stirred for 30 min at room temperature, it was isolated by filtration and recrystallized from pyridine/methanol to give **6** (205 mg, 0.25 mmol) in 50% yield. A crystal suitable for X-ray crystallographic analysis was obtained by recrystallization from pyridine/methanol. Anal. Calcd for $C_{52}H_{57}N_2O_4Fe$: C, 75.26; H, 6.92; N, 3.38. Found: C, 75.06; H, 7.18; N, 3.40. IR (KBr): 3436, 3014, 2952, 2919, 2855, 1608, 1590, 1554, 1459, 1416, 1387, 1331, 1309, 1272, 1226, 1120, 1091, 1060, 1033, 995, 853, 762, 687, 649, 577 cm^{-1}.

7. To a solution of **5** (50 mg, 0.062 mmol) in THF (5 mL) was added a solution of silver perchlorate (15.4 mg, 0.068 mmol) in THF (1 mL). After the mixture was stirred for 30 min at room temperature, it was filtered, and the THF solvent was evaporated in vacuo. The residue, dissolved in CH_2Cl_2, was passed through a Teflon filter (Cosmonice Filter (S), pore size 0.45 μm) to give **7** (49.7 mg, 0.056 mmol). An analytically pure sample was obtained by recrystallization from CH_2Cl_2/hexane. Anal. Calcd for $C_{50}H_{54}N_2O_8$-ClFe: C, 66.56; H, 6.03; N, 3.10. Found: C, 66.41; H, 6.02; N, 3.50. IR (KBr): 3428, 3015, 2955, 2922, 2855, 1608, 1556, 1460, 1422, 1386, 1329, 1304, 1270, 1224, 1121, 1109, 1090, 1062, 985, 855, 759, 691, 651, 579 cm^{-1}.

8. All manipulations were carried out in a glovebox. To a solution of iron(II) acetate (34.8 mg, 0.20 mmol) in deoxygenated methanol (60 mL) was added **24** (143 mg, 0.20 mmol). The solution was heated and was then allowed to stand at room temperature. The resulting red crystalline product was filtered, washed with a small amount of methanol, and dried under an argon atmosphere. **8** was obtained in 55% yield (97 mg, 0.11 mmol). A crystal suitable for X-ray crystallographic analysis was obtained by recrystallization from methanol. Anal. Calcd for $C_{53}H_{62}N_2O_5Fe$: C, 73.77; H, 7.24; N, 3.25. Found: C, 73.92; H, 7.03; N, 3.21.

9. 9 was synthesized from the corresponding chloromanganese complex. To a solution of the chloromanganese complex (21.5 mg, 0.027 mmol) in THF (0.5 mL) was added a solution of silver tetrafluoroborate (6.27 mg, 0.032 mmol) in THF (0.5 mL). After the mixture was stirred for 30 min at room temperature, it was filtered, and the THF solvent was evaporated in vacuo. The residue, dissolved in CH_2Cl_2, was passed through a Teflon filter (Cosmonice Filter (S), pore size 0.45 μm) to give **9** quantitatively (21.0 mg, 0.025 mmol). A crystal suitable for X-ray crystallographic analysis was obtained by recrystallization from CH_2Cl_2/hexane. Anal. Calcd for $C_{50}H_{54}BF_4N_2O_4Mn$: C, 67.57; H, 6.12; N, 3.15. Found: C, 67.26; H, 6.18; N, 3.40. IR (KBr): 3436, 3016, 2965, 2919, 2855, 1607, 1591, 1553, 1461, 1418, 1385, 1330, 1305, 1277, 1223, 1123, 1084, 1064, 1037, 995, 985, 855, 756, 696, 656, 581 cm^{-1}.

Table 6. Crystallographic Data for **5**, **6**, **8**, and **9**

	5	**6**	**8**	**9**
formula	$C_{50}H_{50}ClFeN_2O_2$	$C_{52}H_{56}FeN_2O_4$	$C_{53}H_{59}FeN_2O_5$	$C_{50}H_{52}N_2O_3BF_4Mn$
M_r	802.26	828.87	859.91	870.71
T/K	173	173	173	173
cryst size/mm	0.25 × 0.20 × 0.20	0.40 × 0.20 × 0.15	0.30 × 0.20 × 0.20	0.30 × 0.20 × 0.20
cryst syst	monoclinic	monoclinic	monoclinic	monoclinic
space group	$P2_1/n$ (No. 14)	$P2_1/n$ (No. 14)	$P2_1/n$ (No. 14)	Cc (No. 9)
cryst color	black	black	black	black
a/Å	11.6196(5)	15.643(4)	17.7864(9)	29.053(3)
b/Å	12.7901(5)	11.169(3)	12.9730(5)	8.4182(7)
c/Å	28.174(1)	25.931(7)	20.655(1)	22.860(3)
α/deg				
β/deg	93.438(3)	92.542(3)	103.958(2)	126.620(3)
γ/deg				
V/Å^3	4179.5(3)	4526(2)	4625.2(4)	4487.4(9)
Z value	4	4	4	4
D_{calc}/g cm^{-3}	1.275	1.216	1.235	1.289
GOF	1.86	1.82	2.07	2.01
R1[a]	0.060	0.078	0.066	0.061
wR[b]	0.156	0.178	0.175	0.160

[a] $R1 = \sum||F_o| - |F_c||/\sum|F_o|$. [b] $wR = [\sum w(F_o^2 - F_c^2)^2/\sum w(F_o^2)^2]^{1/2}$.

X-ray Crystallography. Measurements were made on a Rigaku RAXIS−IV Imaging Plate diffractometer or Rigaku/MSC Mercury CCD diffractometer equipped with graphite-monochromated Mo Kα radiation ($\lambda = 0.710\ 70$ Å). Data were collected at 173 K under a cold nitrogen stream. The images were processed with the *CrystalClear* (Rigaku) program.[36] Structures were solved by direct methods with the *TeXsan* crystallographic software.[37] Anisotropic refinement was applied to all non-hydrogen atoms. Hydrogen atoms, except for those of water molecules, were placed at the calculated positions and refined with isotropic parameters. Corrections for Lorentz−polarization effects and absorption were performed. Crystallographic data for each complex are summarized in Table 6. Crystallographic data for **2** is not sufficient, mainly because of the solvent molecules incorporated in the crystal, but is supposed to be valid for discussion on the geometry around the iron center.

DFT Calculations. Electronic structure calculations were carried out using the DFT method in which the B3LYP hybrid functional[38,39] was employed. The *Gaussian98* program[40] was used for the implementation. The ground wave function was described with the LANL2DZ basis set for Fe and Cl where their core electrons were replaced with the effective core potentials.[41] For the other atoms, the (9s5p)/[3s2p] basis sets by Dunning and Hay[42] were used. In the present calculations, spin polarization was taken into account. The spin contaminations in the spin-unrestricted approximation were negligibly small. For example, the expectation values of the $\hat{S}^2$ operator for the Fe^{III}/Cl complex were 3.7944 and 8.7650 for the lowest-spin quartet ($S = {}^3/_2$) and sextet ($S = {}^5/_2$) states, where their deviations from the ideal values were within the tolerance of 1.2%. The number of unpaired electrons in the quartet and sextet states (Table S2 in the supporting Information) indicates that they dominantly localize on the Fe atom and some of them delocalize over the salen ligand. The convergence criteria for geometry optimizations were due to the default values in *Gaussian98*, where the maximum and root-mean-square forces were less than 4.5×10^{-4} and 3.0×10^{-4} au, respectively. The maximum and root-mean-square displacements were 1.8×10^{-3} and 1.2×10^{-3} au, respectively.

Acknowledgment. We thank Prof. T. Yamada for helpful comments on the synthesis of **17**, Dr. Y. Funahashi for assistance in the early stages of the project, Dr. M. Tomura for helpful comments on X-ray crystallographic analysis, and S. Makita for elemental analysis. This work was supported by grants from the Ministry of Education, Culture, Sports, Science and Technology, Japan, and from the Japan Science and Technology Agency, CREST.

Supporting Information Available: ORTEP view and crystallographic data of **2**, X-ray crystallographic files in CIF format for **2**, **5**, **6**, **8**, and **9**, cyclic voltammogram, UV−vis, ^{1}H NMR, EPR, and resonance Raman spectra for **1**−**7**, the resonance Raman spectrum of **3** in the solid state, spin population on the Fe atom in the spin-unrestricted DFT (B3LYP) calculations, and complete ref 40. This material is available free of charge via the Internet at http://pubs.acs.org.

IC060650P

(36) (a) *CrystalClear Software Package*; Rigaku and Molecular Structure Corp.: The Woodlands, TX, 1999. (b) Pflugrath, J. W. *Acta Crystallogr.* **1999**, *D55*, 1718−1725.
(37) *TeXsan*, version 1.11; Rigaku and Molecular Structure Corp.: The Woodlands, TX, 2000.
(38) Becke, A. D. *J. Chem. Phys.* **1993**, *98*, 5648−5652.
(39) Lee, C. T.; Yang, W. T.; Parr, R. G. *Phys. Rev.* **1988**, *B37*, 785−789.
(40) Pople, J. A.; et al. *Gaussian98*, revision A.11.3; Gaussian, Inc.: Pittsburgh, PA, 2002.
(41) (a) Hay, P. J.; Wadt, W. R. *J. Chem. Phys.* **1985**, *82*, 270−283. (b) Wadt, W. R.; Hay, P. J. *J. Chem. Phys.* **1985**, *82*, 284−298. (c) Hay, P. J.; Wadt, W. R. *J. Chem. Phys.* **1985**, *82*, 299−310.
(42) Dunning, T. H., Jr.; Hay, P. J. In *Modern Theoretical Chemistry*; Schaefer, H. F., III, Ed.; Plenum: New York, 1976; Vol. 3, p 1.